The acoustic radiation force of a focused ultrasound beam on a suspended eukaryotic cell

Xiangjun Peng[a,b,f], Wei He[a,b], Fengxian Xin[a,c,*], Guy M. Genin[d,e,f], Tian Jian Lu[b,g,*]

[a] State Key Laboratory for Strength and Vibration of Mechanical Structures, Xi'an Jiaotong University, Xi'an 710049, PR China
[b] State Key Laboratory of Mechanics and Control of Mechanical Structures, Nanjing University of Aeronautics and Astronautics, Nanjing 210016, PR China
[c] MOE Key Laboratory for Multifunctional Materials and Structures, Xi'an Jiaotong University, Xi'an 710049, PR China
[d] Bioinspired Engineering and Biomechanics Center (BEBC), Xi'an Jiaotong University, Xi'an 710049, PR China
[e] The Key Laboratory of Biomedical Information Engineering of Ministry of Education, Xi'an Jiaotong University, Xi'an 710049, PR China
[f] U.S. National Science Foundation Science and Technology Center for Engineering Mechanobiology, and McKelvey School of Engineering, Washington University, St. Louis, MO 63130, USA
[g] Nanjing Center for Multifunctional Lightweight Materials and Structures (MLMS), Nanjing University of Aeronautics and Astronautics, Nanjing 210016, PR China

ARTICLE INFO

ABSTRACT

Although ultrasound tools for manipulating and permeabilizing suspended cells have been available for nearly a century, accurate prediction of the distribution of acoustic radiation force (ARF) continues to be a challenge. We therefore developed an analytical model of the acoustic radiation force (ARF) generated by a focused Gaussian ultrasound beam incident on a eukaryotic cell immersed in an ideal fluid. The model had three layers corresponding to the nucleus, cytoplasm, and membrane, of a eukaryotic cell. We derived an exact expression for the ARF in relation to the geometrical and acoustic parameters of the model cell components. The mechanics of the cell membrane and nucleus, the relative width of the Gaussian beam, the size, position and aspect ratio of the cell had significant influence on the ARF. The model provides a theoretical basis for improved acoustic control of cell trapping, cell sorting, cell assembly, and drug delivery.

1. Introduction

Ultrasound has been applied to manipulate [1] and lyse [2] cells since the 1920s. These were amongst the first contactless particle trapping and manipulation methods in biology and continue to find application in bio-medical research [3,4] A particularly sensitive application of ultrasound manipulation is acoustic tweezers, which has received particular attention due to its advantages in contamination-free and label-free cell handling [5–8]. Numerous experimental, theoretical and numerical studies have demonstrated that acoustic tweezers can be used to align, move and sort microparticles and cells [3,6,9–11]. Higher energy versions of these focused ultrasound technologies can be used to permeabilize membranes to ions and drugs [12–16].

Underlying all of these applications is fine control of acoustic radiation force (ARF). The study of ARF, which is the period-averaged force caused by a sound wave, is just like the optical radiation force generated by electromagneticwaves striking on electrically or magnetically responsive objects [17], therefore has a long history [18]. Investigation of ARF on microparticles dates back to King's theoretical study of ARF on a rigid sphere in an ideal fluid subjected a planar

progressive sound field [19]. Yosioka and Hasegawa extended King's work to compressible spherical particles [20], and extensive subsequent theoretical and experimental works have shown the ARF exerted by a planar acoustic field on a microsphere [21–23] to be very sensitive to the structure and acoustic properties of the micro-particle.

Two theoretical approaches are commonly used to calculate the ARF: the partial-wave expansion method and the ray acoustics method. The ray acoustics method is limited to cases when the wavelength of the acoustic wave is far smaller than the radius of the sphere, but the partial-wave expansion method is applicable to an arbitrary frequency range [24]. The partial-wave expansion method has been used to explore a range of waves in spherical coordinates, including plane waves [20], Bessel waves [25] and Gaussian waves [26].

Gaussian waves are widely used to model optical and acoustical wavefields converging to or diverging from focal regions [26]. Particles can become trapped by a Gaussian wave in the focal region [6]. Focused Gaussian ultrasound waves have found utility in bioscience because they can trap suspended cells for quantification of the cell's mechanical properties [27].

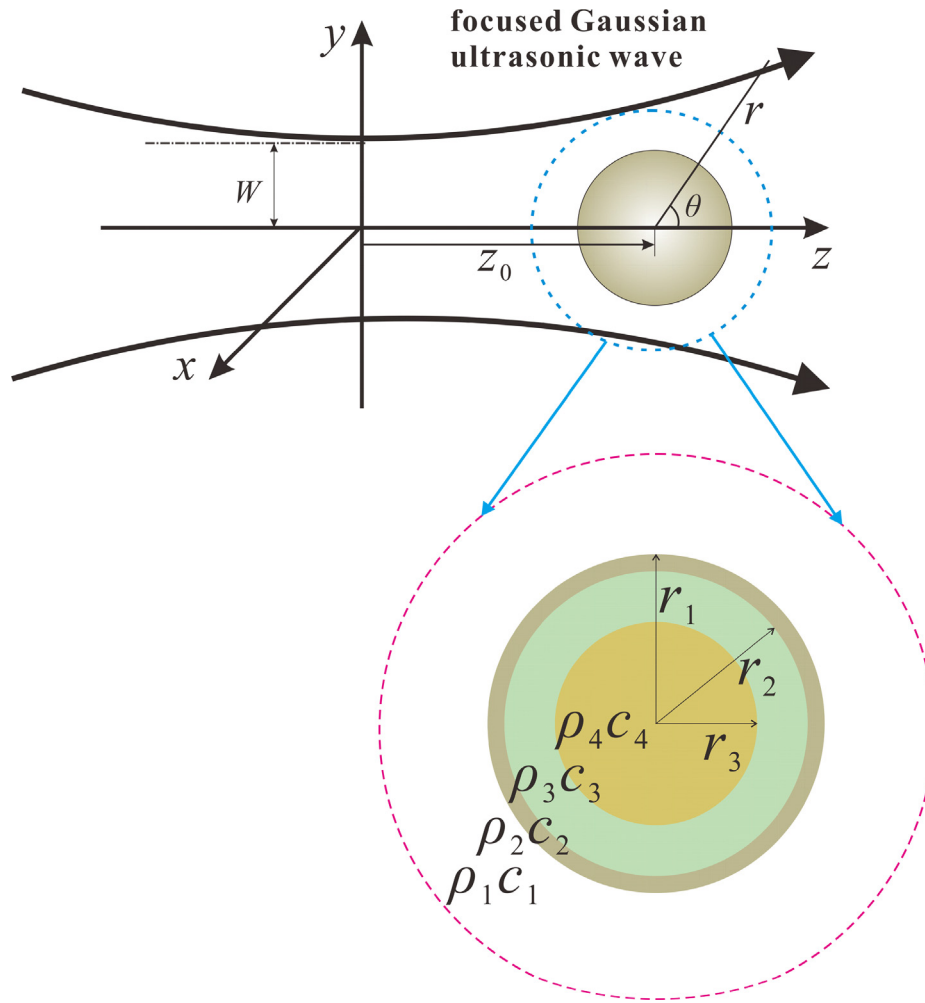In existing theoretical studies of ARF in cell manipulation, cells were

Fig. 1. Schematic of a Gaussian beam incident upon a triple-layered shell (three-layer model) model of a eukaryotic cell.

modeled as homogeneous microspheres [28]. However, eukaryotic cells are heterogeneous, and the nucleus has been reported to affect wave propagation significantly. Thus, the simple homogenous sphere model does not accurately represent eukaryotic cells.

As a first step towards understanding how cell shape and heterogeneity affect ARF, we studied an ellipsoidal cell consisting of a membrane, cytoplasm, and nucleus. This three-layered model was embedded in an ideal fluid that was subjected to a focused Gaussian ultrasound wave. The partial wave expansion method was employed to calculate the ARF on the cell. Results show that the nucleus and membrane play an important role in determining the ARF, along with the aspect ratio of the cell and the size of the cell relative to the Gaussian beam waist.

2. Theoretical model

With reference to Fig. 1, a focused Gaussian ultrasound wave is incident on a eukaryotic cell immersed in an inviscid fluid, with z_0 being the location of the center of the cell relative to the origin of the Cartesian coordination system, which is also the beam waist center. The wave with beam waist radius W propagates along the $+z$ direction. The eukaryotic cell consists of an outer cell membrane with radius r_1, a middle layer (cytoplasm) with radius r_2, and an inner core (cell nucleus) with radius r_3. Let the mass densities and acoustic velocities of the surrounding medium, the cell membrane, the cytoplasm and the nucleus be denoted by (ρ_1, c_1), (ρ_2, c_2), (ρ_3, c_3) and (ρ_4, c_4), respectively. Corresponding acoustic impedances and wave numbers are $Z_i = \rho_i c_i (i = 1, 2, 3, 4)$ and $k_i = \omega/c_i (i = 1, 2, 3, 4)$, ω being the

circular frequency of the Gaussian wave.

In a progressive focused Gaussian ultrasound wave field, the incident wave pressure is expressed by:

$$
\begin{aligned}
&p_i(x, y, z, t) \\
&= \frac{p_0 W}{w(z)} \exp\left[-\frac{(x^2 + y^2)}{w^2(z)}\right] \exp\left\{-i\left\{k\left[\frac{(x^2 + y^2)}{2R(z)} + z\right] - \tan^{-1}\left(\frac{z}{f_C}\right)\right\}\right\} \\
&\quad \exp(-i\omega t)
\end{aligned}
\tag{1}
$$

where $w(z) = W\sqrt{1 + (z/f_C)^2}$ is the beam width, $R(z) = f_C(z/f_C + f_C/z)$ is the radius of curvature of the isophase surface, $\tan^{-1}(z/f_C)$ is the phase factor, and $f_C = kW^2/2$ is the confocal factor.

Although the phase front of the fundamental mode of the incident Gaussian wave is not planar in general, it is very nearly planar in the neighborhood of the beam waist and can be approximated as an acoustic wave with Gaussian amplitude distribution [26]:

$$
p_i(x, y, z, t) \approx p_0 \exp(-(x^2 + y^2)/W^2) \exp(ik_1 z) \exp(-i\omega t)
\tag{2}
$$

We define the wavelength in a particular medium as $\lambda = 2\pi/k_1 = 2\pi c_1/\omega$ and $s = 1/(kW)$. In a spherical coordinate system, with $x = r\sin\theta\cos\varphi$, $y = r\sin\theta\sin\varphi$, $z = r\cos\theta$, the incident acoustic wave pressure may be expanded into a generalized Rayleigh wave series, as:

$$
p_i(r, \theta, t) = p_0 \sum_{n=0}^{\infty} \Lambda_n i^n (2n + 1) j_n(k_1 r_1) P_n(\cos\theta) \exp(-i\omega t)
\tag{3}
$$

where:

$$\Lambda_{2p} = \frac{\Gamma(p+1)}{\Gamma(p+1/2)} \sum_{j=0}^{p} \frac{\Gamma(p+j+1/2)}{(p-j)!j!} Q_0(-4Q_0 s^2)^j \exp(-i\alpha_1 z_0) \tag{4}$$

$$\Lambda_{2p+1} = \frac{\Gamma(p+1)}{\Gamma(p+3/2)} \sum_{j=0}^{p} \frac{\Gamma(p+j+3/2)}{(p-j)!j!} (Q_0 - Q_1 - jQ_1)(-4Q_0 s^2)^j$$
$$\exp(-i\alpha_1 z_0) \tag{5}$$

Here, $Q_0 = 1/(1+2iz_0/l)$, $Q_1 = 2/[\alpha_1 l(i - 2z_0/l)^2]$, $l = \alpha_1 W^2$, $j_n(\cdot)$ is the spherical Bessel function of the first kind, $P_n(\cdot)$ is the Legendre polynomial of order n, and $\Gamma(\cdot)$ is the Gamma function.

The scattered wave field can be expressed as:

$$p_s(r, \theta, t) = p_0 \sum_{n=0}^{\infty} \Lambda_n i^n (2n+1) A_n h_n^{(1)}(k_1 r_1) P_n(\cos\theta) \exp(-i\omega t) \tag{6}$$

in which A_n is the scattering coefficient to be determined by the boundary condition. Therefore, the total wave field outside the three-layer model (eukaryotic cell) takes the form:

$$p_1(r_1, \theta, t)$$
$$= p_0 \sum_{n=0}^{\infty} \Lambda_n i^n (2n+1)[j_n(k_1 r_1) + A_n h_n^{(1)}(k_1 r_1)] P_n(\cos\theta) \exp(-i\omega t) \tag{7}$$

The acoustic wave field in the cell membrane p_2, in the cytoplasm p_3, and in the nucleus p_4 can be expressed as:

$$p_2(r_2, \theta, t)$$
$$= p_0 \sum_{n=0}^{\infty} \Lambda_n i^n (2n+1)[B_n j_n(k_2 r_2) + C_n y_n(k_2 r_2)] P_n(\cos\theta) \exp(-i\omega t) \tag{8}$$

$$p_3(r_3, \theta, t)$$
$$= p_0 \sum_{n=0}^{\infty} \Lambda_n i^n (2n+1)[D_n j_n(k_3 r_3) + E_n y_n(k_3 r_3)] P_n(\cos\theta) \exp(-i\omega t) \tag{9}$$

$$p_4(r_4, \theta, t) = p_0 \sum_{n=0}^{\infty} \Lambda_n i^n (2n+1)[F_n j_n(k_2 r_2)] P_n(\cos\theta) \exp(-i\omega t) \tag{10}$$

where $y_n(\cdot)$ is the spherical Bessel function of the second kind.

To determine the unknown coefficients B_n, C_n, D_n, E_n and F_n, we followed previous researchers in approximating the three layers as having shear resistance that is small compared to their resistance to dilatation [29,30]. Therefore, at their interfaces, the boundary condition was that the velocity and pressure must be continuous, leading to the following form for A_n:

$$A_n$$
$$= -\frac{\rho_2 c_2 j_n'(k_1 r_1)[Q_2 j_n(k_1 r_2) - y_n(k_1 r_2)] - \rho_1 c_1 j_n(k_1 r_1)[Q_2 j_n'(k_1 r_2) - y_n'(k_1 r_2)]}{\rho_2 c_2 h_n^{(1)'}(k_1 r_1)[Q_2 j_n(k_1 r_2) - y_n(k_1 r_2)] - \rho_1 c_1}$$
$$h_n^{(1)}(k_1 r_1)[Q_2 j_n'(k_1 r_2) - y_n'(k_1 r_2)] \tag{11}$$

where

$$Q_1 = \frac{\rho_4 c_4 y_n'(k_3 r_4) j_n(k_4 r_4) - \rho_3 c_3 y_n(k_3 r_4) j_n'(k_4 r_4)}{\rho_4 c_4 j_n'(k_3 r_4) j_n(k_4 r_4) - \rho_3 c_3 j_n(k_3 r_4) j_n'(k_4 r_4)}$$
$$Q_2 = \frac{\rho_3 c_3 [Q_1 j_n(k_3 r_3) - y_n(k_3 r_3)] y_n'(k_2 r_3) - \rho_2 c_2 [Q_1 j_n'(k_3 r_3) - y_n'(k_3 r_3)] y_n(k_2 r_3)}{\rho_3 c_3 [Q_1 j_n(k_3 r_3) - y_n(k_3 r_3)] j_n'(k_2 r_3) - \rho_2 c_2 [Q_1 j_n'(k_3 r_3) - y_n'(k_3 r_3)] j_n(k_2 r_3)} \tag{12}$$

3. Acoustic radiation force

For a continuous focused Gaussian ultrasound wave, the ARF is obtained by integrating the excess of pressure $(p(r, \theta, t) - p_0)$

generated by the sound field over the instantaneous surface $S(t)$ of the sphere, as:

$$\boldsymbol{F}(t) = -\int\int_{S(t)} (p(r, \theta, t) - p_0)\boldsymbol{n}dS \tag{13}$$

where $\boldsymbol{n}$ is the outward normal to $S(t)$. To evaluate the ARF, the excess of pressure should be taken up to second-order terms in the velocity potential. For a periodic wave, the ARF is defined as a time-averaged quantity over period of the sound field. The time-averaged force acting on a sphere immersed in an infinite ideal fluid is:

$$\langle\boldsymbol{F}\rangle = -\int\int_{S(t)} \langle(p - p_0)\rangle\boldsymbol{n}dS$$
$$= -\left\langle \int\int_{S_0} \rho\langle(v_n\boldsymbol{n} + v_t\boldsymbol{t})v_n\rangle\boldsymbol{n}dS \right\rangle$$
$$+ \int\int_{S_0} \left[\frac{1}{2}\frac{\rho}{c^2}\left\langle\left(\frac{\partial\psi}{\partial t}\right)^2\right\rangle - \frac{1}{2}\rho\langle|\nabla\psi|^2\rangle\right]\boldsymbol{n}dS \tag{14}$$

where $\langle\cdot\rangle$ represents the time average, $\boldsymbol{t}$ is an in-plane unit tangential vector of $S(t)$, S_0 is the surface of the target at its equilibrium position, $dS = rdrd\theta$, and the parameters $v_n|_{r=r_1} = -\frac{\partial\psi}{\partial r}$ and $v_t|_{r=r_1} = -\frac{1}{r}\frac{\partial\psi}{\partial\theta}$ are the radial and tangential components of the velocity at the surface, respectively. Here, $\psi = \text{Re}[\phi]$, for which ϕ is the velocity potential expressed as:

$$\phi = \frac{p_1}{-i\omega\rho}$$
$$= \frac{p_0}{-i\omega\rho_1} \sum_{n=0}^{\infty} \Lambda_n i^n (2n+1)[j_n(k_1 r_1) + A_n h_n^{(1)}(k_1 r_1)] P_n(\cos\theta) \exp(-i\omega t) \tag{15}$$

It follows that:

$$\psi = \text{Re}[\phi] = \left|\frac{p_0}{\omega\rho_1}\right| \sum_{n=0}^{\infty} (2n+1)R_n P_n(\cos\theta) \tag{16}$$

$$R_n = \text{Re}(\Lambda_n i^n (U_n + iV_n) \exp(-i\omega t)) \tag{17}$$

in which U_n and V_n are given by:

$$U_n = (1 + \alpha_n)j_n(\alpha_1 r_1) - \beta_n y_n(\alpha_1 r_1)$$
$$V_n = \beta_n j_n(\alpha_1 r_1) + \alpha_n y_n(\alpha_1 r_1) \tag{18}$$

where α_n and β_n are the real part and imaginary part of the scattering coefficient A_n, respectively.

In the direction of wave propagation, the total radiation force on the three-layer model is:

$$\langle F_z\rangle = \langle F_r\rangle + \langle F_\theta\rangle + \langle F_{r,\theta}\rangle + \langle F_t\rangle \tag{19}$$

where

$$\langle F_r\rangle = \left\langle -\pi r_1^2 \rho_1 \int_0^\pi \left(\frac{\partial\psi}{\partial r}\right)_{r=r_1}^2 \sin\theta\cos\theta d\theta \right\rangle \tag{20}$$

$$\langle F_\theta\rangle = \left\langle \pi\rho_1 \int_0^\pi \left(\frac{\partial\psi}{\partial\theta}\right)_{r=r_1}^2 \sin\theta\cos\theta d\theta \right\rangle \tag{21}$$

$$\langle F_{r,\theta}\rangle = \left\langle 2\pi r_1 \rho_1 \int_0^\pi \left(\frac{\partial\psi}{\partial r}\right)_{r=r_1} \left(\frac{\partial\psi}{\partial\theta}\right)_{r=r_1} \sin^2\theta d\theta \right\rangle \tag{22}$$

$$\langle F_t\rangle = \left\langle -\frac{\pi r_1^2 \rho_1}{c_1^2} \int_0^\pi \left(\frac{\partial\psi}{\partial t}\right)_{r=r_1}^2 \sin^2\theta\cos\theta d\theta \right\rangle \tag{23}$$

Substituting Eq. (16) into Eqs. (20)–(23) and using the following equations of time average:

Table 1
Acoustic parameters [29,32]

Material	Density ρ_i (kg/m^3)	Speed of sound c_i (m/s)	Impedance Z_i (MRayl)
Outer layer	970	1450	1.41
Cytoplasm	1000	1508	1.51
Nucleus	1430	1508.5	2.16
Water	1000	1500	1.50

$$\langle R_n R_{n+1} \rangle = \frac{1}{2}[\text{Re}(\Lambda_n \Lambda_{n+1}^*)(U_n V_{n+1} - V_n U_{n+1})$$
$$- \text{Im}(\Lambda_n \Lambda_{n+1}^*)(U_n U_{n+1} + V_n V_{n+1})]$$

$$\langle R_n' R_{n+1}' \rangle = \frac{1}{2}[\text{Re}(\Lambda_n \Lambda_{n+1}^*)(U_n' V_{n+1}' - V_n' U_{n+1}')$$
$$- \text{Im}(\Lambda_n \Lambda_{n+1}^*)(U_n' U_{n+1}' + V_n' V_{n+1}')]$$

$$\langle R_n R_{n+1}' \rangle = \frac{1}{2}[\text{Re}(\Lambda_n \Lambda_{n+1}^*)(U_n V_{n+1}' - V_n U_{n+1}')$$
$$- \text{Im}(\Lambda_n \Lambda_{n+1}^*)(U_n U_{n+1}' + V_n V_{n+1}')]$$

$$\langle R_n' R_{n+1} \rangle = \frac{1}{2}[\text{Re}(\Lambda_n \Lambda_{n+1}^*)(U_n' V_{n+1} - V_n' U_{n+1})$$
$$- \text{Im}(\Lambda_n \Lambda_{n+1}^*)(U_n' U_{n+1} + V_n' V_{n+1})] \tag{24}$$

where the superscript "*" denotes the complex conjugate. We obtain the following components of the radiation force:

$$\langle F_r \rangle = -\frac{2\pi r_1 p_0^2}{\omega^2 \rho_1} \sum_{n=0}^{\infty} \langle R_n' R_{n+1}' \rangle|_{r=r_1} \tag{25}$$

$$\langle F_\theta \rangle = \frac{2\pi r_1 p_0^2}{\omega^2 \rho_1} \sum_{n=0}^{\infty} n(n+1)\langle R_n R_{n+1} \rangle|_{r=r_1} \tag{26}$$

$$\langle F_{r,\theta} \rangle = \frac{2\pi r_1 p_0^2}{\omega^2 \rho_1} \sum_{n=0}^{\infty} [n\langle R_n R_{n+1}' \rangle|_{r=r_1} - (n+1)\langle R_n' R_{n+1} \rangle|_{r=r_1}] \tag{27}$$

$$\langle F_t \rangle = -\frac{2\pi r_1 p_0^2}{\omega^2 \rho_1} \sum_{n=0}^{\infty} \langle R_n R_{n+1} \rangle|_{r=r_1} \tag{28}$$

Upon substituting Eqs. (25)–(28) into Eq. (19), the radiation force on the three-layer model exerted by the incident focused Gaussian wave can be expressed as:

$$\langle F_z \rangle = Y_p F_0 \tag{29}$$

where $F_0 = E_0 A_0$ is characteristic ARF on a cell of cross-sectional area $A_0 = \pi r_1^2$ for a wave with characteristic volumetric energy density $E_0 = p_0^2/(2\rho_1 c_1^2)$, and Y_p is the dimensionless ARF amplification factor that describes the degree to which the shape and heterogeneity of the cell amplify the ARF.

The dimensionless ARF amplification factor, Y_p, is thus the metric used to compare the ARF on different cells. Y_p can be calculated by:

Y_p

$$= -\frac{4}{(\alpha_1 r_1)^2} \sum_{n=0}^{\infty} (n+1)$$
$$\left\{ \begin{array}{l} \text{Re}[\Lambda_n \Lambda_{n+1}^*][\alpha_n + \alpha_{n+1} + 2\alpha_n \alpha_{n+1} + 2\beta_n \beta_{n+1}] \\ + \text{Im}[\Lambda_n \Lambda_{n+1}^*][\beta_{n+1}(1 + 2\alpha_n) - \beta_n(1 + 2\alpha_{n+1})] \end{array} \right\} \tag{30}$$

The series of Eq. (30) can be truncated when $\Lambda_n < 0.0001$. ARF can be obtained by substituting Eqs. (25)–(28) and (30) into Eq. (29).

4. Parametric analyses and numerical simulations

A series of parametric analyses were performed to determine how the dimensionless ARF amplification factor, Y_p, varied with the geometry and composition of cells. Finite element (FE) simulations were performed for many of these to validate the model.

The baseline geometric parameters were chosen to model an oocyte. The outer layer was taken as a homogenization of the corona radiata, zona pellucida, and vitelline membrane, with outer radius $r_1 = 50$ μm and inner radius $r_2 = 45$ μm. Because the nucleus can account for 21–50% of cell volume [31], the outer radius of the nucleus was taken as $r_3 = 30$ μm. Although the position of the nucleus within the cytoplasm of an oocyte can vary, it was modeled as being concentric with the other layers for simplicity.

The Gaussian ultrasound wave beam waist dimension W was set to three times the wavelength ($W = 6\pi c/\omega$) for an acoustic signal with angular frequency ω. The baseline acoustic material parameters used in all graphs and simulations are listed in Table 1.

FE simulations were performed using the commercial FE code COMSOL Multiphysics (COMSOL, Inc., Burlington, MA, USA). Because the Gaussian ultrasound wave field is axisymmetric, the calculation was simplified by taking advantage of axisymmetry. The "pressure acoustics" module of COMSOL was adopted to model wave propagation, and Eq. (1) was used to set the background sound field. The nucleus and surrounding medium of the FE model were meshed with linear, triangular elements, and the swept mesh method was used to create linear quadrilateral meshes for the cytoplasm and cell membrane (Fig. 2). To model an infinite medium surrounding the cell, non-reflecting boundary conditions were used. The "perfectly matched layer" routine in COMSOL was used. A set of elements around the periphery of extracellular medium introduced an acoustic field through pressure boundary conditions, but cancelled acoustic energy that was received back from the medium with minimal reflection back into the medium. Convergence studies were performed to ensure grid independence for each simulation performed. In these, each element edge length was kept smaller than one sixth of the wavelength. Acoustic pressure and velocity fields in the cell and surrounding medium were obtained directly from the FE simulations. Accordingly, based on the numerical results of
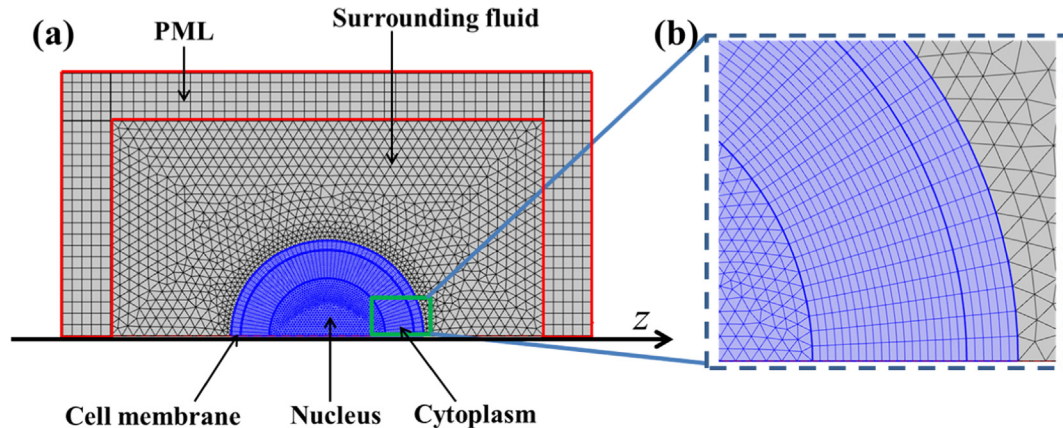

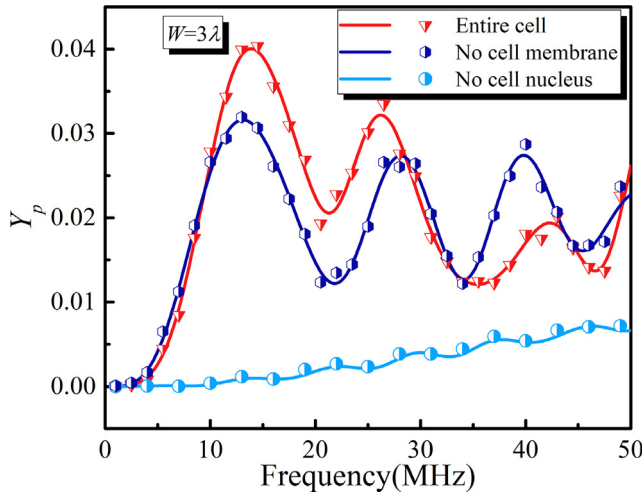**Fig. 2.** Finite element model: (a) representative mesh for eukaryotic cell; (b) enlarged FE mesh.

Fig. 3. Acoustic radiation force amplification factor Y_p as a function of frequency for the three-layer model with $z_0 = 0$. A fictional cell with the acoustic properties of the outer layer changed to match those of the cytoplasm had a response similar to that of the full cell. However, changing the acoustic properties of the nucleus to match those of the cytoplasm attenuated Y_p substantially. Symbols: numerical simulations; curves: theoretical predictions.

sound field, the ARF was calculated by using Eq. (14).

5. Results and discussion

The theoretical and the finite element predictions of the ARF amplification factor Y_p were within a few percent for all cases and acoustic excitation frequencies studied (Fig. 3). For an entire cell (top curve, Fig. 3), Y_p was a nonmonotonic function of excitation frequency, with prominent peaks and dips associated with resonant vibration. The ARF was almost entirely attenuated at low frequencies. We studied how changes to cell geometry, mechanics, and size contributed to the ARF, and how the different components of the cell affected these responses.

5.1. Influence of cell components on ARF

We first asked how the cell membrane and nucleus contributed to the ARF on the entire cell. ARF was greatly attenuated in the absence of a cell nucleus (Fig. 3, plotted for the case of $z_0 = 0$), as would be expected because the acoustic impedance of the nucleus is relatively large compared to that of other cell components (cf. Table 1). This result is consistent with previous observations of backscatter from cells, which is strongly dependent upon the size of the nucleus [31]. By contrast, changing the acoustic properties of the outer layer of the model to match those of the cytoplasm had a relatively effect on the ARF.

5.2. Influence of cell geometry on ARF

The relative sizes of the nuclear and outer layers of the three-layer model affected the magnitude and the frequency dependence of the acoustic radiation force amplification factor Y_p (Fig. 4). In studying these, the focus was the frequency range of 1–20 MHz relevant to standard ultrasound probes, and in particular the peak ARF observed for a spherical cell in the vicinity of 13 MHz (Fig. 3). Note that the several factors are conflated in the contour plots of Fig. 4. As above, the beam waist of the focused Gaussian ultrasound wave was fixed at $W = 3\lambda$. However, because $\lambda = 2\pi/k_1 = 2\pi c_1/\omega$, the size of the beam and hence the relative sizes of these layers change as a function of excitation frequency.

Increasing nuclear radius r_3 while keeping all other dimensions at their baseline values generally increased ARF (Fig. 4a), due to the

relatively high impedance of the nucleus (Table 1) and hence the relatively higher efficiency of scattering. Increasing membrane thickness, $l = r_1 - r_2$, with the outer and nuclear radii fixed at their baseline values also generally increased ARF on the three-layer model (Fig. 4b). Because the contrast between the impedances of the outer layer and the medium is stronger than that between the cytoplasm and surrounding medium (Table 1), replacing cytoplasm with a thicker outer layer, increased the total acoustic scattering of the three-layer model and thus the ARF.

Note that the increases in Y_p are strongly dependent upon frequency. Also, due in part to the conflation of beam waist size and frequency and in part to the vibratory nature of the ARF, certain regions can frequency and size ranges can be found in which an increase in size causes a decrease in ARF. Examples include increasing nuclear radius r_3 beyond 40 μm for an excitation frequency of 12 MHz, and increasing l for an excitation frequency of 7.5 MHz (Fig. 4).

5.3. Influence of acoustic parameters on ARF

With all other parameters held at their baseline levels and again with $W = 3\lambda$, increasing the densities of the layers could increase or decrease the ARF, depending upon the change in contrast of the impedances and upon the vibratory nature of the problem (Fig. 5). Densities were varied ± 20% from baseline values (see Fig. 6).

Increasing the density of the outer layer over this range (776 kg/m³ ≤ ρ_2 ≤ 1160 kg/m³) while holding all other densities at baseline values decreased the ARF (Fig. 5a). This was expected because the outer layer's acoustic impedance became closer to that of the medium and cytoplasm over most of this range (1.12 MRayl ≤ $\rho_2 c_2$ ≤ 1.69 MRayl) (Table 1). A plateau in this trend was reached as the contrast diminished.

Varying the density of the cytoplasm from 800 to 1200kg/m³ led to a non-monotonic change in the ARF (Fig. 5b). As the acoustic impedance of cytoplasm increased over the range 1.20 MRayl ≤ $\rho_3 c_3$ ≤ 1.80 MRayl, the ARF first decreased as acoustic impedance contrast with the outer layer and nucleus decreased, but then increased again as the acoustic impedance surpassed that of the outer layer. Although the impedance contrast with the nucleus decreased steadily over this range, the rise in ARF for higher cytoplasmic densities indicated that the contrast with the outer layer was dominant over this range.

Finally, increasing the density of nucleus from 1144 to 1716 kg/m³ increased the acoustic impedance over 1.73 MRayl ≤ $\rho_4 c_4$ ≤ 2.59 MRayl. Because this corresponded to a steady increase in contrast with the impedance of the cytoplasm, scattering and hence ARF increased monotonically with nuclear density.

Changes of ± 20% to the velocity of sound had effects on the ARF identical to those in Fig. 5. This is expected because acoustic impedance is the product of the velocity of sound and the density within each constituent of the cell, and further confirms that acoustic impedance contrast is the key parameter that governs ARF. This underscores the utility of the present theoretical model in providing guidance for tuning ARF by changing the extracellular medium.

5.4. Influence of the Gaussian beam waist size

Varying the beam waist size, W, had little effect on the amplitude of Y_p, and had no effect on the locations of the frequencies for which ARF exhibited local maxima (Fig. 7). As W increased, the amplitudes increased slightly, although the difference between $W = 5\lambda$ and $W = \infty$ (which is the case of a planar wave) was almost negligible (Fig. 7a). The effects of beam size can be further understood by considering the spatial distribution of the scattered wave field, which follows to form [33]:

$$f_n(f, \theta) = \frac{2}{\alpha_1 r_1} \sum_{n=0}^{\infty} \Lambda_n (2n + 1) A_n P_n(\cos \theta)$$
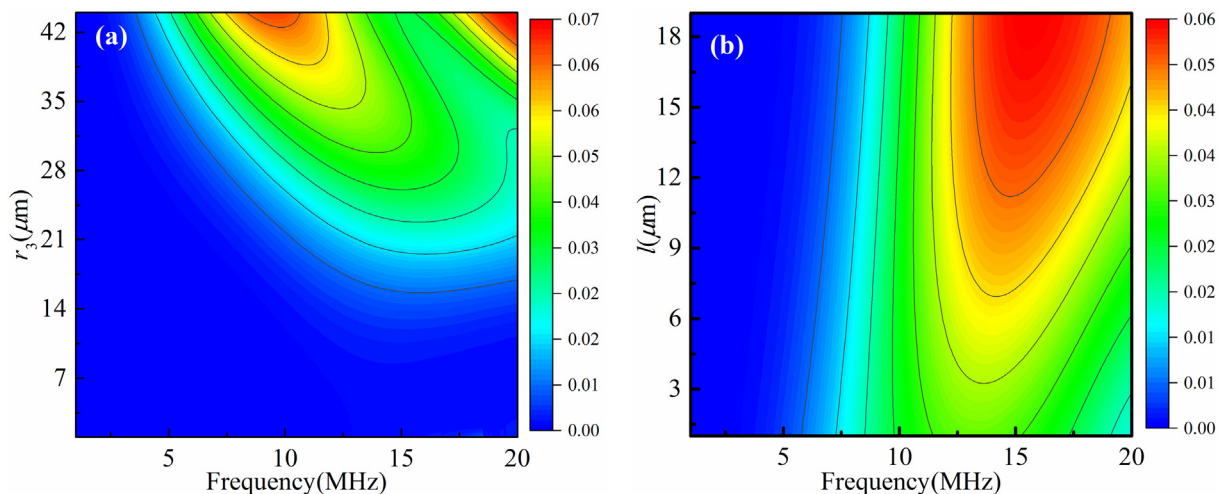
(31)

Fig. 4. Contour plots showing the effects of (a) excitation frequency and nuclear radius, r_3, and (b) excitation frequency and outer layer thickness, $l = r_1 - r_2$, on the acoustic radiation force amplification factor Y_p for a three-layered model. The beam waist of the Gaussian ultrasound wave was fixed at $W = 3\lambda$. Baseline values: $z_0 = 0$, $r_1 = 50\mu$m, $r_2 = 45\mu$m and $r_3 = 30\mu$m.
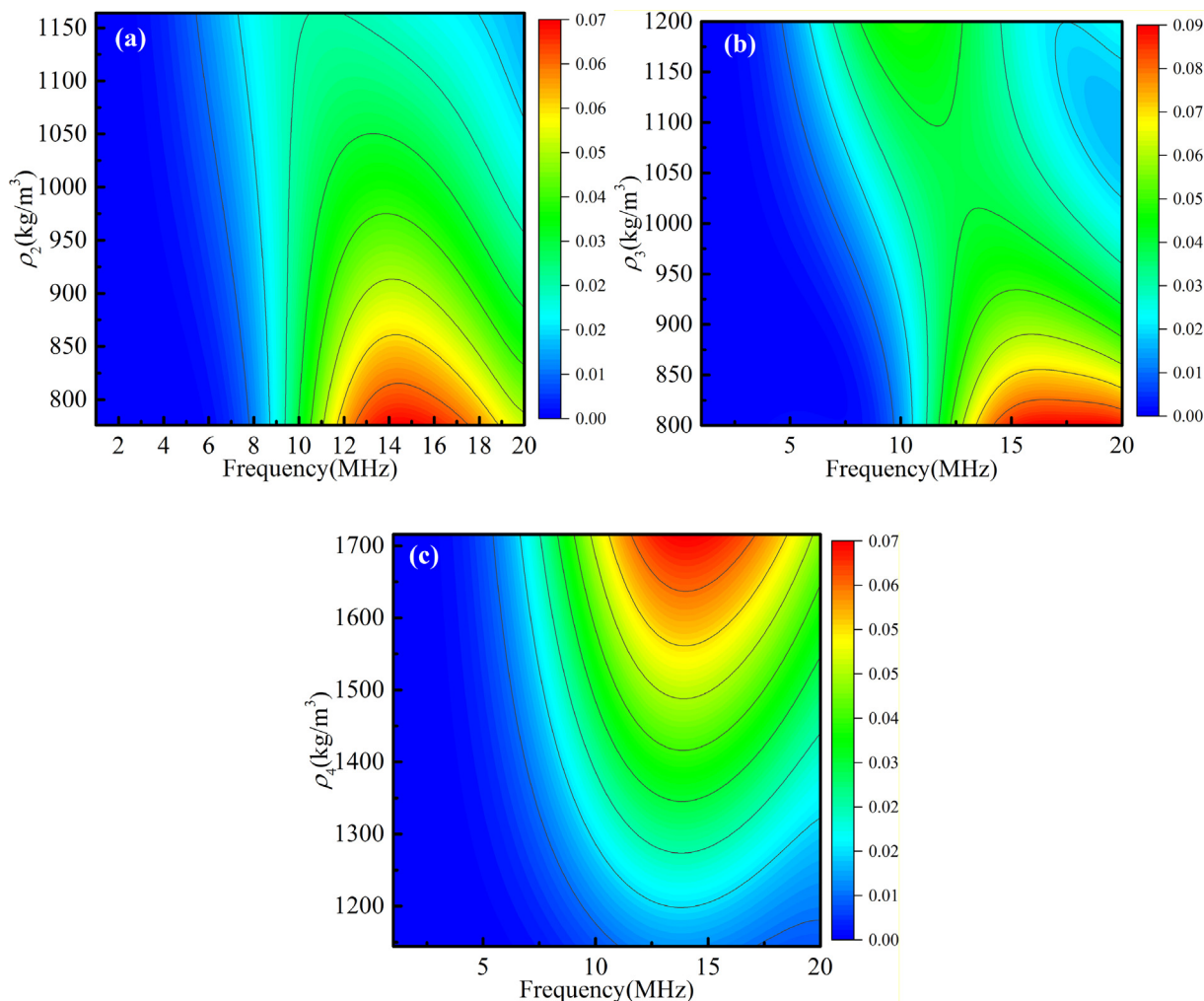

Fig. 5. Contour plots showing the effects on the acoustic radiation force amplification factor of (a) cell membrane density, (b) cytoplasm density and (c) nucleus density. $z_0 = 0$, $W = 3\lambda$, $r_1 = 50\mu$m, $r_2 = 45\mu$m and $r_3 = 30\mu$m.
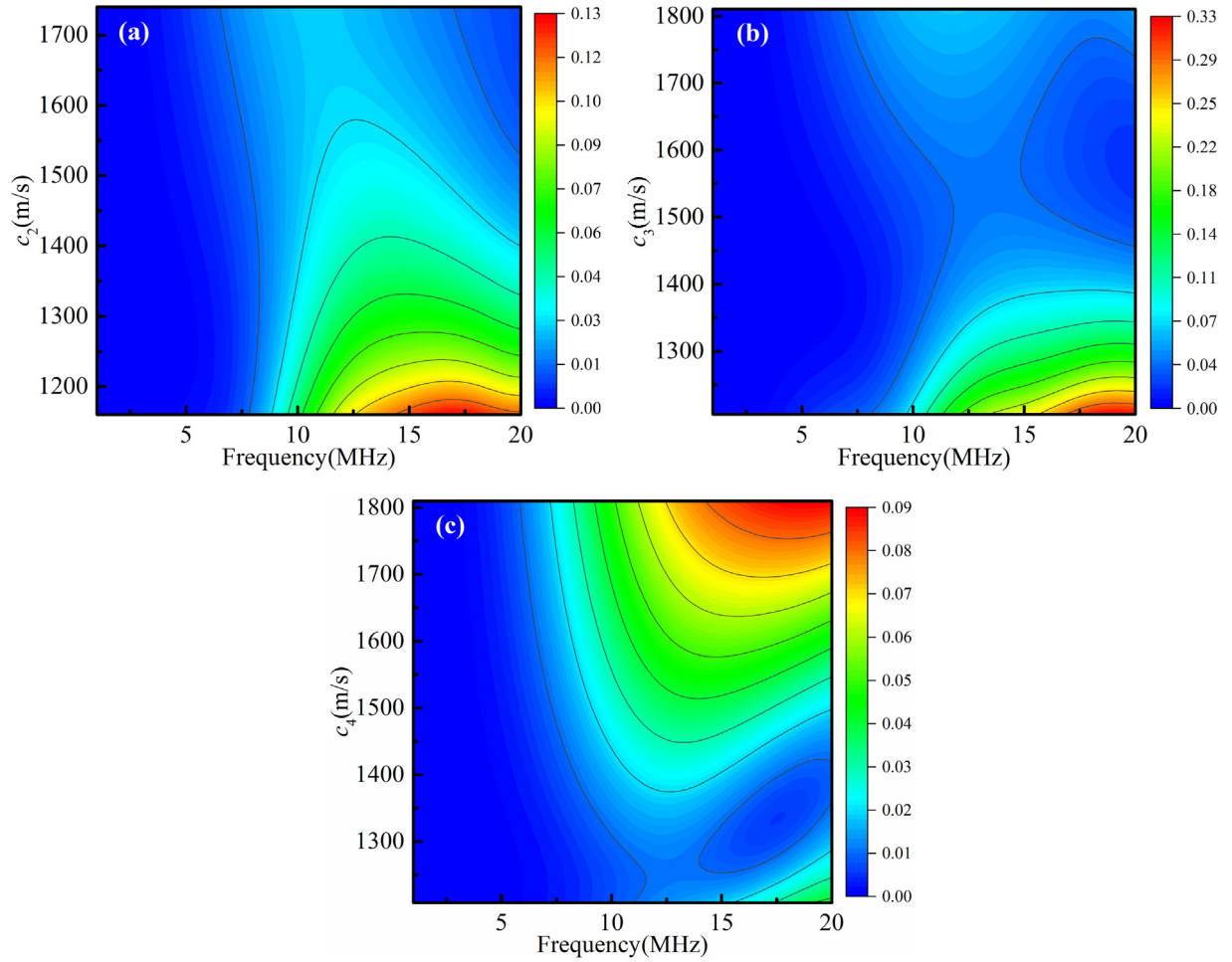
Fig. 6. Contour plots showing the effects on the acoustic radiation force amplification factor of (a) outer layer velocity of sound, (b) cytoplasmic velocity of sound and (c) nuclear velocity of sound. $z_0 = 0$, $W = 3\lambda$, $r_1 = 50\mu m$, $r_2 = 45\mu m$ and $r_3 = 30\mu m$.

For a frequency of 50 MHz, at which the maximum differential was observed in Fig. 7a for $1 \leq W \leq \infty$, the scattered wave amplitude can be seen to increase with beam waist uniformly (Fig. 7b). However, as is evident from the separation of amplitude and angular effects in Eq. (31), the changes in amplitude occur without altering the angular distribution of the scattering.

5.5. Influence of cell size on ARF

The size of the eukaryotic cell affects the acoustic radiation force amplification factor Y_p (Fig. 8a). In studying this, we varied the cell radius r_1 while maintaining the relative dimensions so that the inner radius of the outer layer remained at $r_2 = 0.9r_1$ and the nuclear radius remained at $r_3 = 0.6r_1$. The beam waist of the Gaussian ultrasound wave was fixed at $W = 3\lambda$ (see Figs. 9 and 10).

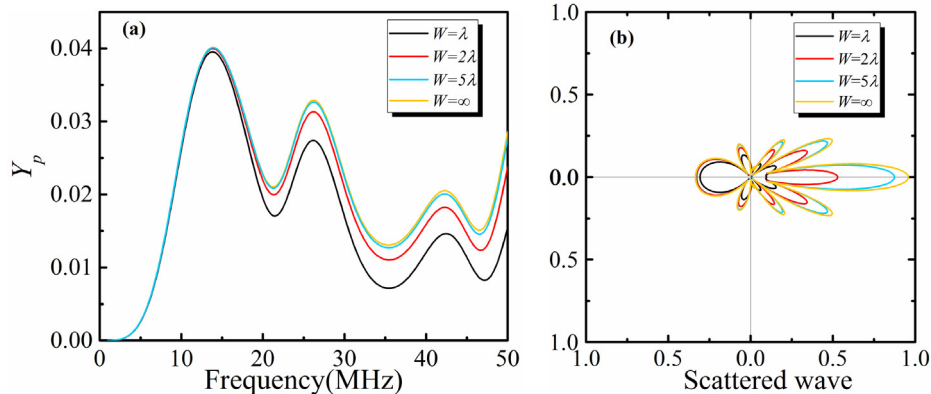The results in Fig. 8 indicate that, as the size of the cell increased,

Fig. 7. (a) Acoustic radiation force function plotted as a function of frequency for selected values of beam waist (eukaryotic cell immersed in water, with $z_0 = 0$, $r_1 = 50\ \mu m$, $r_2 = 45\ \mu m$ and $r_3 = 30\ \mu m$). (b) Angular distribution of the scattered Gaussian ultrasound wave, with frequency fixed at 50 MHz.
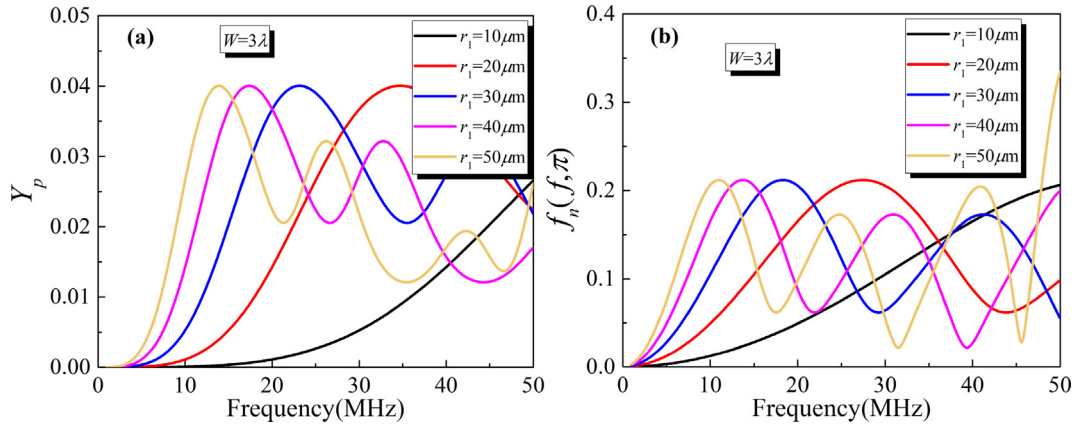
Fig. 8. (a) Acoustic radiation force function plotted as a function of frequency for selected values of cell radius (eukaryotic cell immersed in water, with $z_0 = 0$, $r_2 = 0.9r_1$, $r_3 = 0.6r_1$, $W = 3\lambda$). (b) Backscattering amplitude of the scattered Gaussian ultrasound wave, with beam radius fixed at $W = 3\lambda$.
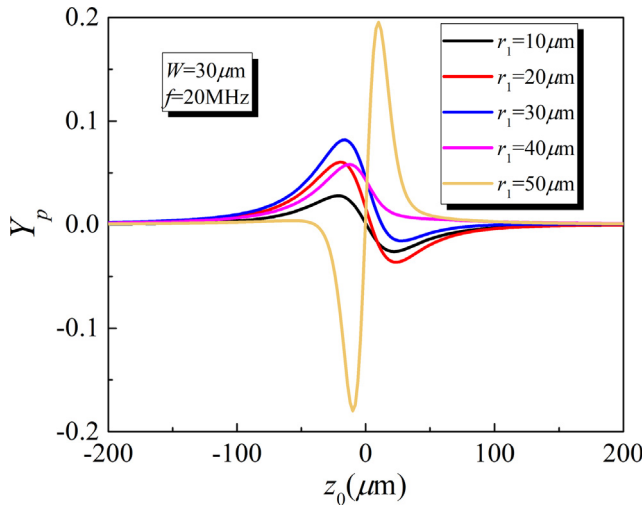

Fig. 9. Acoustic radiation force function plotted as a function of position z_0 for selected values of cell radius (eukaryotic cell immersed in water, with $r_2 = 0.9r_1$, $r_3 = 0.6r_1$, $W = 30\mu$m, and $f = 20$MHz).

the ARF peak shifted to a lower frequency, while the magnitude of this force peak remained constant. For the case of $r_1 = 10 \ \mu$m, this peak was shifted so far that the ARF increased monotonically with frequency over the 50 MHz frequency range studied. For the other cases studied, the resonant frequencies all shifted to lower values with increasing cell size.

The effects of cell size could be further understood by considering the backscattering of the scattered wave, which means that $\theta = \pi$ in Eq. (31). Correspondingly, as the size of the cell increased, the peak of the backscattering amplitude $f_n(f, \pi)$ shifted to a lower frequency without significant change in backscattering amplitude. As a result of this shift, more resonant frequencies and associated peaks appeared for larger cells over the frequency range studied. Based on these theoretical results, for smaller cells with radius ranges from 10 to 20 μm, we need to increase the frequency of the Gaussian ultrasound wave to generate larger ARF.

5.6. Influence of the cell position

The ARF could also be tuned by moving the cell with respect to the ultrasound source. To illustrate this, we calculated the ARF as z_0 was varied in a beam with waist radius W and frequency f fixed at 30 μm and 20 MHz, respectively. The cell studied again had fixed relative dimensions, with the inner radius of outer layer held at $r_2 = 0.9r_1$ and the nuclear radius held at $r_3 = 0.6r_1$.

The highly focused Gaussian ultrasound wave generated negative ARF for certain values of z_0, in an "acoustic tweezer" effect analogous to the phenomenon underlying optical tweezers. This arises from the competition between the two forces that comprise the ARF: a gradient force, which is negative and arises due to the high gradient of the extracellular sound wave field; and a scattering force, which is positive. For example, for a small cell with $r_1 = 10\mu$m, a positive peak and a negative valley were found for $z_0 = -22\mu$m and $z_0 = 24\mu$m, respectively. Here, the gradient force is dominant over the scattering force and thus the ARF is negative for $z_0 = 24\mu$m. A similar phenomenon can be observed for the cells with $r_1 = 20\mu$m and $r_1 = 30\mu$m. However, for the cell with $r_1 = 40\mu$m, the gradient force cannot countervail the scattering force and thus only positive ARF exists, which means that this kind of cell cannot be trapped by a single focused Gaussian ultrasound wave.

For a large cell with $r_1 = 50\mu$m, we find that negative ARF appears for $z_0 < 0$, which differs from the trend observed for smaller cells. This highlights the central role that the cell position z_0 plays in determining both the sign and magnitude of the ARF. Results also provide a predictive framework for tuning a highly focused Gaussian ultrasound wave for use as acoustic tweezers.

5.7. Influence of the cell shape on ARF

Although scattering by ellipsoidal objects is challenging to study analytically, the problem is of interest because most cells elongate upon spreading. We therefore used the FE model to consider two kinds of ellipsoidal three-layer models: prolate and oblate spheroids. The cell had an axis of axisymmetry aligned with the centerline of a focused acoustical Gaussian beam and was centered in the beam waist. Due to this symmetry, the ARF exists without any acoustic radiation torque. The partially enlarged view of the three-layer model is shown in Fig. 8b, with the cell membrane and cytoplasm thickness being 5μm and 15μm. With the reference to Fig. 8 c, the ARF is sensitive to the aspect ratio b/a. Prolate spheroids (higher b/a, with the long axis parallel to the beam axis) have dramatically larger peak ARF. For oblate spheroids, sensitivity to aspect ratio is smaller. The reason for this is that a larger value of aspect ratio b/a means a larger curvature on the illuminated side, leading to enhanced acoustic scattering and ARF.

6. Conclusions

An analytical model has been developed to predict the acoustic radiation force (ARF) generated by a focused Gaussian ultrasound beam incident on a spherical three-layered shell (three-layer model) immersed in ideal fluid. The method of finite series is employed, with the Gaussian progressive wave simulated using spherical harmonic
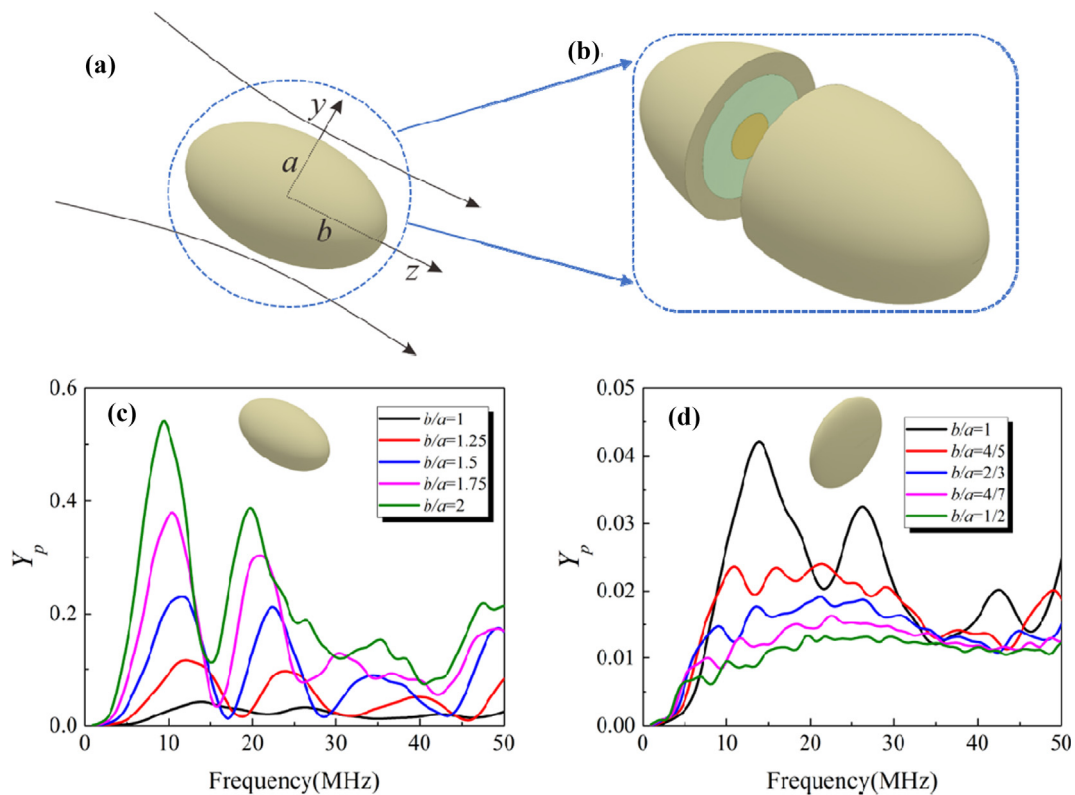
Fig. 10. Acoustic radiation force amplification factor plotted as a function of frequency for spheroids of varying aspect ratio. (a) Schematic of a Gaussian beam incident upon a spheroidal three-layer model. (b) Cross-sectional view of the spheroidal three-layer model. (c) Frequency dependence of the ARF amplification factor of a prolate three-layer model generated by a focused Gaussian wave, for several values of aspect ratio b/a. (d) Frequency dependence of the ARF amplification factor of oblate three-layer models, showing values of ARF an order of magnitude lower than those of the prolate cells in panel.

functions. The model is subsequently used to calculate the ARF on a eukaryotic cell suspended freely in a focused progressive Gaussian ultrasound wave. Finite element simulations are performed to validate the proposed model, with good agreement achieved. Main conclusions drawn are:

(1) As the cell membrane thickness or nucleus radius is increased, the ARF increases distinctly.
(2) The impedance of each constituent of the cell plays an important role in affecting the ARF: increasing the impedance of cell membrane reduces the ARF; as the impedance of cytoplasm is increased, the ARF decreases first and then increases; increasing the impedance of cell nucleus leads to enhanced ARF.
(3) The influence of the beam width of the Gaussian ultrasound wave on the ARF is significant only when it is relatively small.
(4) The size of the cell can significantly affect the peaks of the ARF. Larger cells show more resonant frequencies and hence more ARF peaks in the 1–50 MHz range of excitation frequencies.
(5) The sign and magnitude of the ARF can be tuned by adjusting the position z_0 of the cell relative to the ultrasound transducer. This arises from a competition between the negative gradient force and the positive scattering force.
(6) The aspect ratio b/a (= major axis/minor axis) of the spheroid three-layer model significantly affects the ARF.

The results presented in this study provide theoretical basis for the further development of acoustic control technology for cell trapping/ sorting/assembling and drug delivery applications.

Declaration of Competing Interest

The authors declare that they have no known competing financial interests or personal relationships that could have appeared to influence the work reported in this paper.

References

[1] F.O. Schmitt, Ultrasonic micromanipulation, Protoplasma 7 (1929) 332–340.
[2] E.N. Harvey, E.B. Harvey, A.L. Loomis, Further observations on the effect of high frequency sound waves on living matter, Biol. Bull. 55 (1928) 459–469.
[3] F. Guo, et al., Three-dimensional manipulation of single cells using surface acoustic waves, Proc. Natl. Acad. Sci. U.S.A. 113 (2016) 1522.
[4] G. Bao, S. Suresh, Cell and molecular mechanics of biological materials, Nat. Mater. 2 (2003) 715–725.
[5] X. Ding, et al., Surface acoustic wave microfluidics, Lab Chip 13 (2013) 3626–3649.
[6] M.G. Kim, et al., Label-free analysis of the characteristics of a single cell trapped by acoustic tweezers, Sci. Rep. 7 (2017).
[7] J.R. Wu, Acoustical tweezers, J. Acoust. Soc. Am. 89 (1991) 2140–2143.
[8] J. Lee, et al., Transverse acoustic trapping using a Gaussian focused ultrasound, Ultrasound Med. Biol. 36 (2010) 350–355.
[9] F.G. Mitri, Acoustic radiation force on a sphere in standing and quasi-standing zero-order Bessel beam tweezers, Ann. Phys. 323 (2008) 1604–1620.
[10] P. Li, et al., Acoustic separation of circulating tumor cells, Proc. Natl. Acad. Sci. U.S.A. 112 (2015) 4970–4975.
[11] P.L. Marston, Axial radiation force of a Bessel beam on a sphere and direction reversal of the force, J. Acoust. Soc. Am. 120 (2006) 3518–3524.
[12] J. Liu, T.N. Lewis, M.R. Prausnitz, Non-invasive assessment and control of ultrasound-mediated membrane permeabilization, Pharm. Res. 15 (1998) 918–924.
[13] K. Tachibana, T. Uchida, K. Ogawa, N. Yamashita, K. Tamura, Induction of cell-membrane porosity by ultrasound, Lancet 353 (1999) 1409–1409.

[14] J. Sundaram, B.R. Mellein, S. Mitragotri, An experimental and theoretical analysis of ultrasound-induced permeabilization of cell membranes, Biophys. J. 84 (2003) 3087–3101.

[15] L.J.M. Juffermans, P.A. Dijkmans, R.J.P. Musters, C.A. Visser, O. Kamp, Transient permeabilization of cell membranes by ultrasound-exposed microbubbles is related to formation of hydrogen peroxide, Am. J. Physiol.-Heart Circ. Physiol. 291 (2006) H1595–H1601.

[16] A. van Wamel, et al., Vibrating microbubbles poking individual cells: Drug transfer into cells via sonoporation, J. Control. Release 112 (2006) 149–155.

[17] X. Peng, W. He, Y. Liu, F. Xin, T.J. Lu, Optomechanical soft metamaterials, Acta Mech. Sin. 33 (2017) 575–584.

[18] M. Rajabi, M. Behzad, An exploration in acoustic radiation force experienced by cylindrical shells via resonance scattering theory, Ultrasonics 54 (2014) 971–980.

[19] L.V. King, On the acoustic radiation pressure on spheres, Proc. Roy. Soc. London 147 (1934) 212–240.

[20] T. Hasegawa, K. Yosioka, Acoustic-radiation force on a solid elastic sphere, J. Acoust. Soc. Am. 46 (1969) 1139.

[21] J. Chen, X. Liu, J. Liu, Y. Mao, P.L. Marston, Acoustic radiation force on a sphere in a progressive and standing zero-order quasi-Bessel-Gauss beam, Ultrasonics 76 (2017) 1–9.

[22] T. Hasegawa, Acoustic radiation force on a sphere in a quasistationary wave field–theory, J. Acous. Soc. Am. 65 (1979) 32–40.

[23] B. Diego, T. Jean-Louis, M. Régis, Three-dimensional acoustic radiation force on an arbitrarily located elastic sphere, J. Acous. Soc. Am. 133 (2013) 25–36.

[24] R. Wu, et al., Acoustic radiation force on a double-layer microsphere by a Gaussian focused beam, J. Appl. Phys. 116 (2014) 569.

[25] M. Azarpeyvand, Acoustic radiation force of a Bessel beam on a porous sphere, J. Acous. Soc. Am. 131 (2012) 4337–4348.

[26] X. Zhang, G. Zhang, Acoustic radiation force of a Gaussian beam incident on spherical particles in water, Ultrasound Med. Bio 38 (2012) 2007–2017.

[27] J.Y. Hwang, et al., Cell deformation by single-beam acoustic trapping: a promising tool for measurements of cell mechanics, Sci. Rep. 6 (2016) 27238.

[28] L.H. Ford, Estimate of the vibrational frequencies of spherical virus particles, Phys. Rev. E 67 (2003) 051924.

[29] R.E. Baddour, M.D. Sherar, J.W. Hunt, G.J. Czarnota, M.C. Kolios, High-frequency ultrasound scattering from microspheres and single cells, J. Acoust. Soc. Am. 117 (2005) 934–943.

[30] A. Han, R. Abuhabsah, R.J. Miller, S. Sarwate, W.D. O'Brien Jr., The measurement of ultrasound backscattering from cell pellet biophantoms and tumors ex vivo, J. Acous. Soc. Am. 134 (2013) 686–693.

[31] R.E. Baddour, M.C. Kolios, The fluid and elastic nature of nucleated cells: Implications from the cellular backscatter response, J. Acoust. Soc. Am. 121 (2007) EL16-EL22.

[32] Y.Y. Wang, J. Yao, X.W. Wu, D.J. Wu, X.J. Liu, Influences of the geometry and acoustic parameter on acoustic radiation forces on three-layered nucleate cells, J. Appl. Phys. 122 (2017).

[33] J.J. Faran, Sound scattering by solid cylinders and spheres, J. Acoust. Soc. Am. 23 (1951) 405–418.